Journal of Power Sources 199 (2012) 239–246

Contents lists available at SciVerse ScienceDirect

Journal of Power Sources

journal homepage: www.elsevier.com/locate/jpowsour

Development of ionic liquid-based lithium battery prototypes

G.-T. Kim [a], S.S. Jeong [a], M.-Z. Xue [a], A. Balducci [a], M. Winter [a], S. Passerini [a,*], F. Alessandrini [b], G.B. Appetecchi [b,**]

[a] University of Muenster, Institute of Physical Chemistry, Corrensstr. 28/30, D48149 Münster, Germany
[b] ENEA, Agency for New Technologies, Energy and Sustainable Economic Development, UTRINN-IFC, Via Anguillarese 301, Rome 00123, Italy

ARTICLE INFO

Article history:
Received 14 July 2011
Received in revised form 4 October 2011
Accepted 11 October 2011
Available online 17 October 2011

Keywords:
Ionic liquid
Solvent-free electrolyte
Sodium carboxymethylcellulose
Lithium polymer battery prototype

ABSTRACT

The lab-scale manufacturing of Li/$LiFePO_4$ and $Li_4Ti_5O_{12}$/$LiFePO_4$ stacked battery prototypes and their performance characterization are described here. The prototypes were realized in the frame of an European Project devoted to the development of greener and safer lithium batteries, based on ionic liquid electrolytes, for integration with photovoltaic panels. *N*-Butyl-*N*-methylpyrrolidinium bis(trifluoromethanesulfonyl)imide (PYR_{14}TFSI) and *N*-butyl-*N*-methylpyrrolidinium bis(fluoromethanesulfonyl)imide (PYR_{14}FSI), selected as the ionic liquids (ILs), were used to formulate the poly(ethylene oxide)-$LiN(SO_2CF_3)_2$-PYR_{14}TFSI (PEO-LiTFSI-PYR_{14}TFSI) polymer electrolyte and the LiTFSI-PYR_{14}FSI liquid electrolyte, which were employed to produce lithium metal and lithium-ion prototypes, respectively. The composite electrodes for the lithium metal and lithium-ion prototypes were prepared through, respectively, a solvent-free and a water-based procedure route. The performance of the lithium battery prototypes was evaluated in terms of specific capacity, energy, cycle life and coulombic efficiency at different current densities. The results have indicated high reproducibility and the feasibility of scaling-up solvent-free, lithium batteries based on ionic liquids for low and mid rate applications such as renewable energy storage.

1. Introduction

Ionic liquids (ILs), organic/inorganic salts generally molten at room temperature, represent a very interesting new class of room temperature fluids since their non-flammability, negligible vapor pressure in conjunction with remarkable ionic conductivity, high thermal, chemical and electrochemical stability, high heat capacity and, in some cases, hydrophobicity [1]. Because of these unique properties ILs are excellent candidates as electrolytes and/or electrolyte components to replace volatile and hazardous organic solvents (alkyl carbonates) in lithium batteries.

Ionic liquids based on saturated, cyclic, quaternary ammonium cations as *N*-alkyl-*N*-methyl-pyrrolidinium (PYR_{1A} where the subscripts indicates the number of carbons in the alkyl side chains, alkyl = n-propyl, n-butyl), and bis(trifluoromethanesulfonyl)imide (TFSI) or bis(fluoromethanesulfonyl)imide (FSI) as the anion have been successfully proposed for use in lithium batteries since their sub-ambient melting temperature, high room temperature conductivity, suitable electrochemical stability [2–5]. The last characteristic originates from the absence of acidic protons and double bounds that would strongly deplete the electrochemical stability and compatibility with the lithium metal anode [2,6,7]. Therefore, LiX-PYR_{1A}X (X = FSI or TFSI, A = propyl, n-butyl) mixtures have been extensively investigated, showing very good cycling reversibility into lithium [8] and graphite [9–12] anodes, and $LiCoO_2$ cathodes [13]. Particularly, PYR_{14}FSI-LiTFSI mixtures have been recently employed as electrolytes in $Li_4Ti_5O_{12}$/$LiFePO_4$ lithium-ion cells, which have displayed very good cycling performance [14,15].

Moreover, it was successfully demonstrated [16–19] that the incorporation of PYR_{1A}TFSI ionic liquids (mainly PYR_{14}TFSI) into solid polymer electrolytes (SPEs) largely enhances the room temperature ionic conductivity (above 10^{-4} S cm^{-1} at 20 °C) while maintaining wide electrochemical stability and good compatibility towards the lithium metal anode even after prolonged storage times. The addition of ionic liquids allowed reducing the operative temperature of lithium metal polymer batteries (LMPBs) without depleting their performance [20–22]. Recently, it was shown that UV cross-linking allows incorporating higher ionic liquid amounts into the polymer electrolyte, thus further enhancing the ionic conductivity (e.g., 3.7×10^{-4} S cm^{-1} at 20 °C) without depleting its electrochemical and mechanical properties [23].

In this scenario, we decided to investigate the scale-up of lithium cells based on two different chemistries: (i) Li/$LiFePO_4$ (*high energy*)

* Corresponding author. Tel.: +49 251 8336026; fax: +49 251 8336032.
** Corresponding author. Tel.: +39 06 3048 3924; fax: +39 6 3048 6357.
E-mail addresses: stefano.passerini@uni-muenster.de (S. Passerini), gianni.appetecchi@enea.it (G.B. Appetecchi).

0378-7753/$ – see front matter © 2011 Elsevier B.V. All rights reserved.
doi:10.1016/j.jpowsour.2011.10.036

lithium metal polymer cells using an UV cross-linked PEO-LiTFSI-$PYR_{14}TFSI$ membrane as the electrolyte and, (ii) $Li_4Ti_5O_{12}/LiFePO_4$ (*room temperature*) lithium-ion cells using a $PYR_{14}FSI$-LiTFSI electrolyte mixture. The objective was to realize greener and safer lithium cell prototypes having a capacity up to 1 A h for low-mid rate applications such as renewable energy storage. The use of non-flammable, non-volatile, ionic liquid-based (polymer or not) electrolytes is, in fact, expected to largely improve the safety of lithium battery systems. For the Li-ion prototype, the safety level results further enhanced by the use of lithium titanate (instead lithium metal) as anode active material. $Li_4Ti_5O_{12}/LiFePO_4$ cells are considered among the safest, if not the safest, lithium-ion battery chemistry. In addition, it should be pointed that the composite electrodes were made using the fluorine-free, water-soluble, natural binder carboxymethylcellulose sodium salt (CMC) instead of the more expensive and less environmentally friend polyvinylidendi-fluoride (PVdF). Thus, the lithium-ion electrode manufacturing involved the use of water as the only solvent [14,15] in the place of the hazardous, toxic and much more expensive N-methylpyrrolidone (NMP). The use of CMC allows not only low cost and environmentally friend manufacturing processes but also easier recycle of the battery components. The dissolution in water of the binder allows, for example, a full recovery of the metallic current collectors [14,15].

In the present paper we report the characteristics and the cycling performance of rechargeable, $Li/LiFePO_4$ (LMPB) and $Li_4Ti_5O_{12}/LiFePO_4$ (LIB) stacked battery prototypes.

2. Experimental

2.1. Synthesis of ionic liquid materials

The *N*-butyl-*N*-methylpyrrolidinium bis(trifluoromethanesulfonyl)imide, $PYR_{14}TFSI$, and *N*-butyl-*N*-methylpyrrolidinium bis(fluoromethanesulfonyl)imide, $PYR_{14}FSI$, ionic liquids were synthesized through a procedure route developed at ENEA [24,25]. The chemicals *N*-methylpyrrolidine (ACROS, 98 wt%) and 1-bromobutane (Aldrich, 99 wt%) were previously purified through activated carbon (Aldrich, Darco-G60) and alumina (Aldrich, acidic, Brockmann I) before the synthesis process. The LiTFSI (3 M, 99.9 wt%) and KFSI salts (99.9 wt%, Dai-ichi Kogyo, Seiyaku Co., Ltd, Japan), activated carbon, alumina and ethyl acetate (Aldrich, >99.5 wt%) were used as received. The synthesized ionic liquids exhibited water content below 2 ppm and other impurities below 100 ppm as determined by Karl-Fischer, ICP-OES and ion chromatography techniques.

2.2. Preparation of cross-linked PEO electrolytes and lithium metal cell cathodes

A solvent-free, hot-pressing process developed at ENEA [23] was followed to prepare the cross-linked PEO-LiTFSI-$PYR_{14}TFSI$ ternary solid polymer electrolytes and the $LiFePO_4$ composite cathodes. The process was performed in a very low relative humidity dry room (R.H. < 0.1% at 20 °C). For the SPE samples, LiTFSI (3 M, 99.9 wt%) and $PYR_{14}TFSI$ were dried under vacuum at 120 °C for at least 18 h before use while poly(ethylene oxide) (PEO, Dow Chemical, WSR 301, M_W = 4,000,000) was dried at 50 °C for 48 h. Benzophenone (Bp, Aldrich) was used (as received) as the initiator for the cross-linking process. The Bp/PEO weight ratio was kept equal to 0.05 [23] while the $(PYR_{14})^+/Li^+$ mole ratio was fixed equal to 2 [23]. Firstly, Bp was dissolved in $PYR_{14}TFSI$ by heating under vacuum. PEO and LiTFSI (EO/Li mole ratio = 10) [19] were mixed in a mortar and, then, added to the Bp/$PYR_{14}TFSI$ solution. After complete blending, the PEO-LiTFSI-$PYR_{14}TFSI$-Bp mixture was annealed under vacuum at 100 °C for several hours to obtain a homogeneous, plastic-like material. The latter was sandwiched between two Mylar foils and, then, hot-pressed at 70 °C and 180 kg cm^{-2} for 7–8 min to obtain thin tapes of about 0.1 mm thickness. Finally, the polymer electrolyte tapes (9.0 cm × 6.0 cm) were cross-linked by UV irradiation (UV Karl-Suss MA 45 photo-irradiator equipped with a 350 W Hg lamp) for 8 min (4 min for each side). The final weight composition of the cross-linked electrolytic tapes was 35.0 wt% PEO, 10.0 wt% LiTFSI and 55.0 wt% $PYR_{14}TFSI$.

Cross-linked, composite, cathode tapes were prepared by intimately mixing carbon-coated $LiFePO_4$ (43% in weight, Süd Chemie, average particle size: 0.3 μm, carbon content: 2.3 wt%) and carbon (KJB, Akzo Nobel, 7 wt%) which were previously dried in a vacuum oven at 120 °C for at least 24 h. PEO, LiTFSI and $PYR_{14}TFSI$ were dried as well as for the SPE tapes. Then, PEO (17.5 wt%), LiTFSI (5.0 wt%) and $PYR_{14}TFSI$ (27.5 wt%) and Bp (Bp/PEO weight ratio = 0.05) were separately mixed to obtain a paste-like mixture, which was added to the previous $LiFePO_4$/C blend. The final cathodic mixture was firstly vacuum annealed at 100 °C overnight and, then, cold-calendared to form about 0.05 mm thick cathode films. Finally, the cathode tapes (8.0 cm × 5.0 cm) were UV photo-irradiated for 8 min (4 min on each side) by using a Karl-Suss MA 45 equipment. The active material mass loading approaches 4.5 mg cm^{-2}, corresponding to 0.75 mA h cm^{-2} (e.g., considering the $LiFePO_4$ theoretical capacity equal to 170 mA h g^{-1}). The composite cathodes as well as the cross-linked electrolytes exhibited a water content below 20 ppm.

2.3. Preparation of lithium-ion cell electrodes

Carbon-coated $LiFePO_4$ (average particle size: 0.3 μm, carbon content: 2.3 wt%) and uncoated $Li_4Ti_5O_{12}$ (average particle size: 2 μm), both provided by Süd Chemie, were used as received. Sodium-carboxymethylcellulose (CMC, Dow Wolff Cellulosics, Walocel CRT 2000 PPA 12) with a degree of substitution of 1.2 was used as the binder whereas Super-P carbon (TIMCAL, average particle size: 30 nm) was used as the electronic conducting agent. $LiFePO_4$ and $Li_4Ti_5O_{12}$ electrodes were prepared following a common recipe [14,15]. CMC was firstly dissolved in deionized water by magnetic stirring at room temperature. The required amount of Super-P was then added to the aqueous solution containing CMC and the resulting mixture was ball milled in a zirconia jar loaded with 5 mm zirconia balls. The mixing was performed for more than 1 h with a planetary ball miller (Fritsch, Pulverisette 4; rotation speed: 800 rpm). The selected amount of active material was then added to the mixture and the resulting slurry was homogenized by ball milling at room temperature for one additional hour. During the preparation of the lithium titanate anodes, 0.025 g of formic acid per gram of active material was introduced to neutralize (pH = 7) the slurry, which had a very basic character, in order to prevent corrosion phenomena at aluminium current collectors. The so-formed slurries were cast onto both the faces of Al foils (30.0 cm × 15.0 cm, 20 μm thick, purity >99.9%) by using a laboratory scale blade coater to obtain double-side coated electrodes. A pre-drying in an atmospheric oven with stagnant air at 80–100 °C for 1 h was applied after coating each side of the current collector. Double-side coated electrodes having an overall electrochemically active area of 80 cm^2 (8.0 cm × 5.0 cm each face) were cut and, finally, dried at 180 °C under vacuum for 24 h. The dry material composition of the cathode was 88 wt% $LiFePO_4$, 8 wt% Super-P and 4 wt% CMC whereas that of the anodes was 87 wt% $Li_4Ti_5O_{12}$, 8 wt% Super-P and 5 wt% CMC. The dry thickness of the cathode and anode materials was about 40 μm on each side of the current collector corresponding to an average active material mass loading ranging from about 5.0 mg cm^{-2} to 5.5 mg cm^{-2}, i.e., corresponding to a capacity of 0.85–0.95 mA h cm^{-2} by considering the

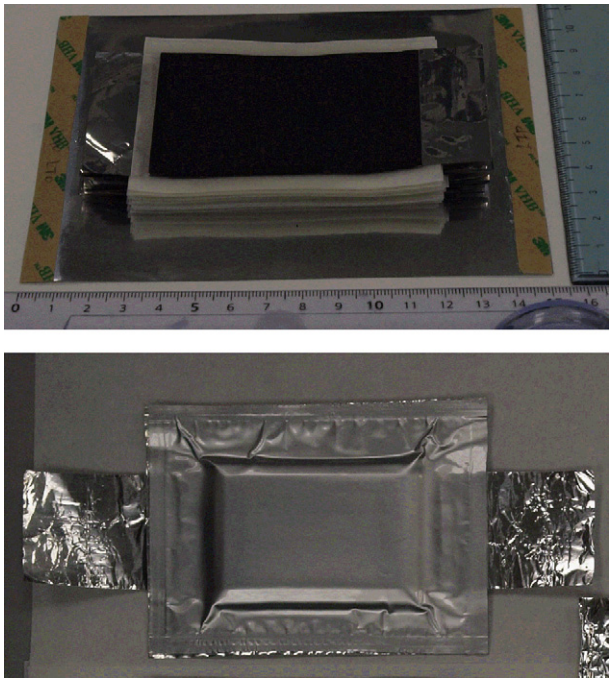

Fig. 1. Picture of a scaled-up, ionic liquid-based, $Li_4Ti_5O_{12}$/$LiFePO_4$ LIB prototype before (upper panel) and after housing in vacuum-sealed pouch-bag (lower panel).

theoretical capacity of $LiFePO_4$ and $Li_4Ti_5O_{12}$ equal to 170 mA h g^{-1} and 175 mA h g^{-1}, respectively.

2.4. Lithium battery prototype manufacturing

The lithium battery prototypes were assembled in the dry-room by stacking from twelve to fourteen double-side coated electrodes (see upper picture in Fig. 1) to achieve a theoretical capacity ranging from 0.7 A h to 0.8 A h. In Table 1 are illustrated the characteristics (i.e., unit number, size, density and weight) of the prototype components.

The manufacturing of the LMPB prototypes involved firstly the realization of double-side cathodic half-cells, each of them made by placing a $LiFePO_4$ composite electrode tape (8.0 cm × 5.0 cm) onto both faces of an aluminium foil current collector (10.0 cm × 5.0 cm × 0.0025 cm). The current collector extended by 2 cm the length of the cathode tape to allow the electrical connection with the positive tab. Then, two polymer electrolyte tapes (9.0 cm × 6.0 cm × 0.01 cm) were used to complete the double-side cathodic half-cell. The electrolyte layers exceeded the active material tape on each side (by 0.5 cm) to avoid short circuits with the lithium metal anodes. The LMPB prototypes were assembled stacking, alternatively, twelve bipolar cathode half-cells and thirteen lithium metal tapes (10.0 cm × 5.0 cm × 0.005 cm). The anode and cathode current collectors were welded to one Al° and Cu° tab (5.0 cm × 5.0 cm × 0.003 cm), respectively. Successively, the prototypes were kept (20 °C) under vacuum overnight to remove the gas trapped at electrolyte/electrode interface, thus improving the electrode contact.

The LIB prototypes were manufactured stacking, alternatively, fifteen bipolar $LiFePO_4$ cathodes, twenty eight separators (9.0 cm × 6.0 cm glass fiber tapes) and fourteen $Li_4Ti_5O_{12}$ anodes (Fig. 1). During the stacking, the separators and electrodes were progressively loaded with LiTFSI-$PYR_{14}FSI$ electrolyte (mole ratio equal to 1:9, corresponding to a weight ratio of 1:10.1). Vacuum was applied step by step to promote the penetration of the electrolyte into the separator and electrode pores. Each prototype was loaded

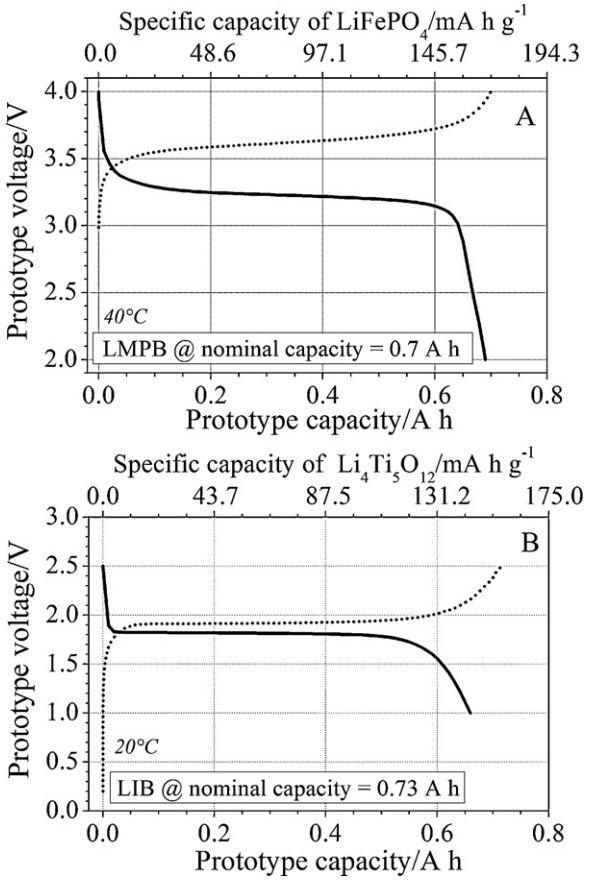

Fig. 2. Voltage vs. capacity profile of the 1st charge-discharge cycle for a scaled-up, ionic liquid-based, Li/$LiFePO_4$ LMPB (panel A) and $Li_4Ti_5O_{12}$/$LiFePO_4$ LIB prototype (panel B). *Current rate*: C/20. In the upper axis is indicated the capacity of the $LiFePO_4$ (panel A) and of the $Li_4Ti_5O_{12}$ electrode (panel B) for the LMPB for the LIB prototype, respectively.

with an overall electrolyte volume equal to 25 ml (e.g., 33.5 g). Two aluminium tabs were welded to the anode and cathode current collectors.

Successively, the stacked LMPB and LIB prototypes were housed in soft packages, which were evacuated for about 1 h and heat-sealed under vacuum. Fig. 1 shows pictures of a scaled-up, battery prototype before (upper panel) and after housing in vacuum pouch-bag (lower panel), respectively.

2.5. Electrochemical tests

The cycling tests on the LMPB and LIB prototypes were performed in the 2.0–4.0 V (LMPB) and 1.0–2.5 V (LIB) voltage range, respectively, by means of a Maccor S4000 battery tester at current densities ranging from 0.035–0.040 mA cm^{-2} (C/20) to 1.4–1.6 mA cm^{-2} (2C). Each discharge step was run at the same current rate adopted for the previous charge half-cycle. The performance of the battery prototypes was evaluated in terms of capacity, energy, cycle life and coulombic efficiency at 20 °C (LIB) and 40 °C (LMPB) using climatic chambers (Binder GmbH MK53).

3. Results and discussion

In Fig. 2 is plotted the voltage vs. capacity profile of the first charge-discharge cycle (C/20) of Li/$LiFePO_4$ (panel A, j = 0.035 mA cm^{-2}) and $Li_4Ti_5O_{12}$/$LiFePO_4$ (panel B, j = 0.040 mA cm^{-2}) prototypes held at 40 °C (LMPB) and 20 °C (LIB), respectively. As expected, the voltage profiles are characterized

Table 1
Characteristics of the scaled-up, ionic liquid-based, Li/$LiFePO_4$ lithium polymer and $Li_4Ti_5O_{12}$/$LiFePO_4$ lithium-ion prototype components. The size and the weight of the final devices are also reported. (*) = geometrical density. (**) = weight percent considering the weight of the electrolyte and separators.

Component	Characteristic	LMPB prototype	LIB prototype
Anode	Unit number	13	28
	Size, cm	10.0 × 5.0 × 0.005	8.0 × 5.0 × 0.004
	Density, g cm^{-3}	0.53	1.20 (*)
	Weight, g	1.72	5.19
	Percent in weight	3.9	7.6
Electrolyte	Unit number	24	28
	Size, cm	9.0 × 6.0 × 0.01	9.0 × 6.0 × 0.01
	Density, g cm^{-3}	1.60	–
	Weight, g	20.74	39.94
	Percent in weight	47.6	58.2 (**)
Cathode	Unit number	24	30
	Size, cm	8.0 × 5.0 × 0.005	8.0 × 5.0 × 0.005
	Density, g cm^{-3}	2.00	1.1
	Weight, g	9.6	6.60
	Percent in weight	22.0	9.6
Anode collector	Unit number	–	14
	Size, cm	–	10.0 × 5.0 × 0.0025
	Density, g cm^{-3}	–	2.70
	Weight, g	–	4.76
	Percent in weight	–	7.0
Cathode collector	Unit number	12	15
	Size, cm	10.0 × 5.0 × 0.0025	10.0 × 5.0 × 0.0025
	Density, g cm^{-3}	2.70	2.70
	Weight, g	4.08	5.10
	Percent in weight	9.4	7.4
Anode tab	Unit number	1	1
	Size, cm	5.0 × 5.0 × 0.003	5.0 × 5.0 × 0.003
	Density, g cm^{-3}	8.89	2.70
	Weight, g	0.67	0.20
	Percent in weight	1.5	0.3
Cathode tab	Unit number	1	1
	Size, cm	5.0 × 5.0 × 0.003	5.0 × 5.0 × 0.003
	Density, g cm^{-3}	2.70	2.70
	Weight, g	0.20	0.20
	Percent in weight	0.5	0.3
Package	Unit number	2	2
	Size, cm	15.0 × 11.0 × 0.01 2.00	15.0 × 11.0 × 0.01
	Density, g cm^{-3}	2.00	2.00
	Weight, g	6.60	6.60
	Percent in weight	15.1	9.6

by well-defined, smooth plateaus related to the very reversible, 2-phase insertion processes in $LiFePO_4$ and $Li_4Ti_5O_{12}$ [14,23]. The cathode-limited LMPB prototype displayed the full theoretical capacity (0.7 A h) in the initial charge up to 4.0 V (corresponding to 1 equiv. of Li per mole of $LiFePO_4$ or 170 mA h g^{-1}). In the following discharge step, 98.6% of the lithium removed, e.g., 0.69 A h (corresponding to 167.6 mA h per gram of $LiFePO_4$), was inserted. On the other hand, the anode-limited LIB prototype was capable of storing only 0.73 A h (nominal capacity), corresponding to 91% of the theoretical value (0.9 equiv. of Li per mole of $Li_4Ti_5O_{12}$ or 158 mA h g^{-1}). It is to note, however, that the nominal capacity in $Li_4Ti_5O_{12}$/$LiFePO_4$ cells was found to be close to 160 mA h per gram of $Li_4Ti_5O_{12}$ (instead of the theoretical 175 mA h g^{-1}) [14]. In the following discharge half-cycle, about 92% of the lithium inserted in $Li_4Ti_5O_{12}$ was removed. Overall, the experimental capacity of the LIB prototype at C/20 (during the 1st discharge half-cycle) was 0.66 A h, corresponding to 146.2 mA h per gram of $Li_4Ti_5O_{12}$, instead of the expected 0.8 A h. However, it is very important to notice the very modest difference in voltage (about 100 mV) between the charge and discharge plateaus, which indicates a rather high energy efficiency of the electrical storage due, among other factors, to a low charge transfer resistance at the electrolyte/electrode interfaces.

Fig. 3A illustrates the discharge curves of a LMPB prototype cycled at various current densities (40 °C). The test was performed subjecting the prototype to a sequence charge/discharge cycles at C/20, C/10, C/5, C/3, C/2, and 1C rate (the current density ranged from 0.035 mA cm^{-2} (C/20) to 0.7 mA cm^{-2} (1C)). As seen in Fig. 2, the LMPB prototype was capable to discharge almost the full capacity (0.70 A h) at C/20. However, a progressive change of the discharge curve was observed upon increasing current rates. The increase of the initial ohmic drop and of the slope of the plateau, due to conductivity and diffusion limitations in the polymer electrolyte, were the cause of the cell performance decrease. The discharge capacity was found to substantially decrease from 0.69 A h at C/20 to 0.11 A h at C/2, i.e., for a current increase of one order of magnitude. At higher rates (≥1C), only very modest reversible capacities (<0.05 A h) were delivered by the prototype. The delivered capacity vs. current density dependence of two LMPB prototypes tested at 40 °C is reported in panel B and Table 2. The results show a very good reproducibility of the two cells (and, thus, of the prototype manufacturing) but they also evidence the pronounced decreasing trend with the current density.

Fig. 4 reports the long-term performance of a LMPB prototype in terms of discharge capacity (panel A) and coulombic efficiency (panel B). The test was performed repeating the multi-rate sequence described above. In the C/20 cycles, the cell delivered 91% (0.64 A h), 86% (0.6 A h) and 67% (0.47 A h) of the initial capacity at the 600th, 800th, and 1000th cycle, respectively. Apart for an initial capacity decay, the scaled-up Li/$LiFePO_4$ prototypes showed a very stable cycling performance up to 600 cycles. The coulombic efficiency (panel B of Fig. 4) is seen to be close to 99% for 700

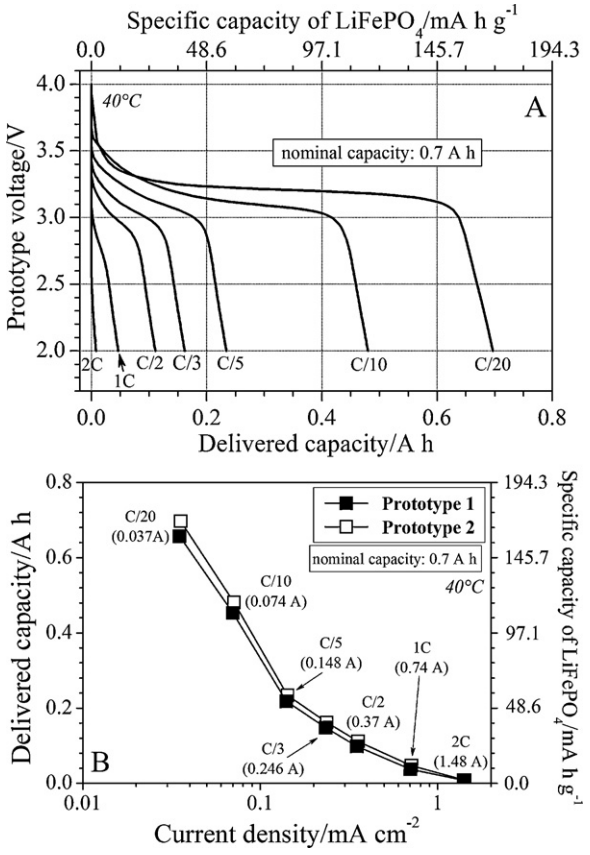

Fig. 3. Voltage vs. discharge capacity profiles (panel A) and discharge capacity vs. current density dependence (panel B) of scaled-up, ionic liquid-based, Li/LiFePO$_4$ LMPB prototypes. The capacity was also reported with respect to the LiFePO$_4$ active material weight for comparison purpose. The average discharge current values (and the corresponding discharge rates) are also indicated in the panels. $T = 40\,^{\circ}C$.

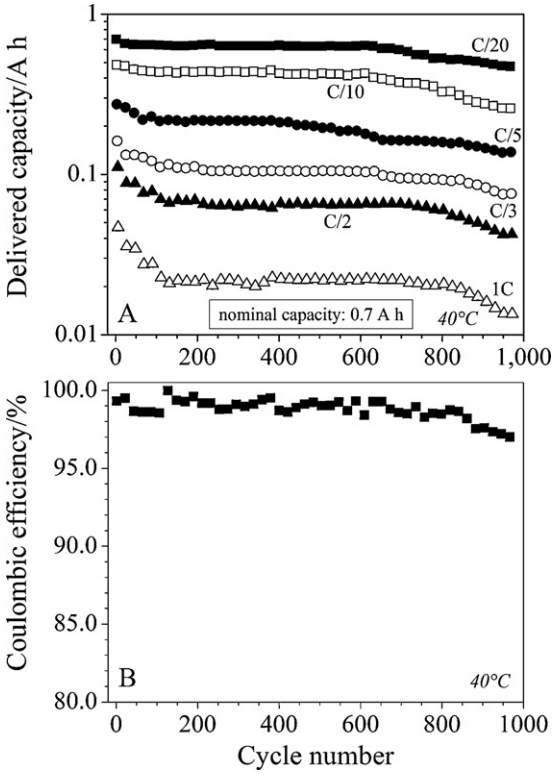

Fig. 4. Discharge capacity (panel A) and coulombic efficiency (panel B) evolution of a scaled-up, ionic liquid-based, Li/LiFePO$_4$ LMPB prototype at different current rates. $T = 40\,^{\circ}C$.

charge/discharge cycles with a progressive decrease in the following cycles. Overall, this result supports for a very good reversibility of the Li$^+$ plating/stripping process in cross-linked PEO-LiTFSI-PYR$_{14}$TFSI polymer electrolytes [23]. In addition, no evidence of dendritic growth appeared during the cycling.

The results of the electrochemical tests performed on the Li$_4$Ti$_5$O$_{12}$/LiFePO$_4$ (LIB) prototypes subjected to the multi-rate testing protocol (see description above) at 20 °C, are reported in Figs. 5 and 6. The low rate discharge curves (C/20 and C/10) (Fig. 5A) show a very flat plateau, which is typical of the LiFePO$_4$ and Li$_4$Ti$_5$O$_{12}$ materials [14]. However, a fast progressing increase of the voltage plateau slope is seen at rates higher than C/5, resulting in a fast decrease in capacity. In fact, while about 0.66 A h (more than 90% of the nominal capacity value) was delivered at C/20, only 0.08 A h was provided at C/2. This corresponds to almost a ten times capacity decrease for a ten-fold current density increase. It is important to notice, however, the very modest increase of the ohmic drop in passing from C/20 to 2 C that supports for a good ionic conductivity of the LiTFSI-PYR$_{14}$FSI electrolyte mixture. The discharge capacity evolution of two Li$_4$Ti$_5$O$_{12}$/LiFePO$_4$ LIB prototypes as a function of the current density is reported in panel B (Fig. 5) and Table 2. Once more, the data supports for the good reproducibility of the manufacturing process of the LIB stacked prototypes. The capacity vs. current density plot is characterized by three different linear trends, which may be associated with three distinguished regions:

(i) a low current rate region ($j \leq 0.08\,mA\,cm^{-2}$) where the delivered capacity is limited by the diffusion phenomena taking place within the electrode active material phase [26–28];
(ii) an intermediate current rate region ($0.08\,mA\,cm^{-2} < j \leq 0.27\,mA\,cm^{-2}$) which is characterized by a more pronounced slope of the capacity vs. current density curve. The more remarkable decrease in capacity (from 0.48 A h to 0.16 A h) is due to the limitation originating from diffusive phenomena occurring in the ionic liquid-based electrolyte (LiFSI-PYR$_{14}$FSI) [26–28];
(iii) a third region ($j > 0.27\,mA\,cm^{-2}$) in which the delivered capacity is less than 10% of the total capacity but its decrease upon increasing rate is very moderate. This behavior can be mainly ascribed to the intercalation of the Li$^+$ ion present in the pores of the electrodes only. Nominally, no contribution from the Li$^+$ ion diffusion in the bulk electrolyte is existing in this current regime.

The long-term performance (at 20 °C) of the scaled-up Li$_4$Ti$_5$O$_{12}$/LiFePO$_4$ prototypes is also reported in Fig. 6 where are displayed the voltage vs. capacity profile of selected

Table 2
Discharge capacity values of the scaled-up, ionic liquid-based, Li/LiFePO$_4$ LMPB prototype and Li$_4$Ti$_5$O$_{12}$/LiFePO$_4$ LIB prototype at different current rates. $T = 40\,^{\circ}C$ (LMPB) and 20 °C (LIB).

Current density, mA cm^{-2}		Rate	Delivered capacity, A h			
LMPB	LIB		LMPB		LIB	
			#1	#2	#1	#2
0.035	0.040	C/20	0.657	0.690	0.660	0.656
0.070	0.080	C/10	0.453	0.481	0.602	0.582
0.140	0.160	C/5	0.218	0.234	0.354	0.366
0.233	0.270	C/3	0.148	0.162	0.106	0.105
0.350	0.400	C/2	0.098	0.111	0.083	0.081
0.700	0.800	1C	0.037	0.047	0.061	0.055
1.400	1.600	2C	0.008	0.008	0.041	0.037

charge/discharge cycles at C/20 (panel A) and the capacity vs. cycle evolution (panel B). Once more, the test was performed repeating the multi-rate charge/discharge sequence with current densities ranging from 0.04 mA cm^{-2} (C/20) to 1.6 mA cm^{-2} (2 C). The cell voltage vs. capacity behavior in Fig. 6A indicates the efficient electrochemical energy storage in this cell. In fact, the voltage difference between the charge and discharge plateau remains nominally constant over 1000 cycles. In addition, the LIB prototype showed a very good capacity retention even at high rates (Fig. 6B), apart for an initial decay observed at C/5 rate. For instance, the prototype delivered more than 72% of the initial capacity (C/20) at the 973rd cycle (0.51 A h). This result, which is in full agreement with those reported for CMC-based, $Li_4Ti_5O_{12}$ and $LiFePO_4$ half-cells (lithium metal anode) upon prolonged cycling tests [15], supports for a very good cycling performance of the scaled-up prototypes, and for the feasibility of LiTFSI-PYR_{14}FSI mixtures as electrolytes in $Li_4Ti_5O_{12}$/$LiFePO_4$ batteries. The performance decay recorded at the intermediate rate (C/5) is to be associated with the electrode morphology and electrolyte availability in the cell. It should be considered, in fact, that the capacity delivered at this intermediate rate shows a very strong change (see Fig. 5 panel B). Nevertheless, the overall long-term cycling performance of the lab-made prototypes is certainly interesting considering its scale (0.7 A h), the still poor development of ionic liquid-based electrolytes, and the use of a natural binder in both electrodes. An inspection, run on a few Li/LFP and LTO/LFP stacked prototypes, has shown a very good vacuum retention after 1000 charge/discharge cycles, this suggesting no appreciable gas development (due to electrochemical decomposition) when the batteries are on. Also, no phase separation and/or visual degradation of the ionic liquid electrolyte was observed whereas no relevant oxidation was detected at the internal current collectors.

Table 3
Specifications of the scaled-up, ionic liquid-based, Li/$LiFePO_4$ lithium polymer and $Li_4Ti_5O_{12}$/$LiFePO_4$ lithium-ion prototypes. (*) = without tabs and package.

Specification	LMPB prototype	LIB prototype
Single cells	12	14
Size, cm	12.0 × 6.0 × 0.475	12.0 × 6.0 × 0.747
Active area, cm^2	960 (40 × 2 × 12)	1120 (40 × 2 × 14)
Nominal voltage, V	3.4	1.8
Overall anode weight, g	1.72	5.19
Anode active material weight, g	1.72	4.52
Anode capacity, A h	6.54	0.79
Overall cathode weight, g	9.60	6.60
Cathode active material weight, g	4.13	5.81
Cathode capacity, A h	0.70	0.99
OCV (as assembled), V	3.03	0.20
Overall weight, g	43.61 (36.14*)	68.59 (61.59*)
Theoretical capacity, A h	0.70	0.79
Specific energy, W h kg^{-1}	54.6	20.7

The specifications of the scaled-up Li/$LiFePO_4$ and $Li_4Ti_5O_{12}$/$LiFePO_4$ cell prototypes are summarized in Table 3. The length (12.0 cm) and the height (6.0 cm) are analogous for both prototypes whereas the thickness was 0.455 cm for the LMPB and 0.727 cm for the LIB. The weight of the LMPB and LIB prototypes was 43.61 g (39.31 g excluding tabs and package) and 68.59 g (61.59 g), respectively. The prototypes had a theoretical capacity from 0.7 A h (LMPB, cathode limited) to 0.8 A h (LIB, anode limited). Considering the nominal discharge voltages of 3.4 V (LMPB) and

Table 4
Size, average weight and weight fraction of the components of the scaled-up, ionic liquid-based, Li/$LiFePO_4$ and $Li_4Ti_5O_{12}$/$LiFePO_4$ lithium battery prototypes fabricated as reported in this work and upon further optimization. (*) = referred to the single component unit. (**) = referred to an active material content increase up to 60.0 wt% (from 43.0 wt%), which would increase the $LiFePO_4$ electrode loading and prototype capacity up to 1.04 mA h cm^{-2} and 0.98 A h, respectively. (***) = referred to two-fold thicker $LiFePO_4$ electrode (electrode loading equal to 1.7–1.9 mA h cm^{-2}), which would correspond to an increase in capacity, overall weight and thickness of the prototype up to 1.6 A h, 37.0 g and 0.591 cm, respectively.

	LMPB prototype as fabricated			Optimized LMPB prototype		
	(*) size, cm	wt, g	wt fraction, %	(*) size, cm	wt, g	wt fraction, %
Anodes	10.0 × 5.0 × 0.005	1.72	3.9	8.5 × 5.0 × 0.001	0.39	2.6
Electrolyte separators	9.0 × 6.0 × 0.01	20.74	47.6	8.2 × 5.2 × 0.001	1.63	11.0
Cathodes	8.0 × 5.0 × 0.005	9.60	22.0	8.0 × 5.0 × 0.005	9.60	64.5
Anode collectors	–	–	–	–	–	–
Cathode collectors	10.0 × 5.0 × 0.0025	4.08	9.4	8.5 × 5.0 × 0.001	1.38	9.3
Anode tab	5.0 × 5.0 × 0.003	0.67	1.5	5.0 × 0.5 × 0.002	0.04	0.3
Cathode tab	5.0 × 5.0 × 0.003	0.20	0.5	5.0 × 0.5 × 0.002	0.01	0.1
Package	15.0 × 11.0 × 0.01	6.60	15.1	13.0 × 7.0 × 0.005	1.82	12.2
Final device	12.0 × 6.0 × 0.475	43.61	100.0	9.0 × 5.2 × 0.179	14.87	100.0
Specific energy, W h kg^{-1}			54.6			160.1 (224.1)**
Volumetric energy, W h dm^{-3}			69.5			284.1 (397.7)**
	LIB prototype as fabricated			Optimized LIB prototype		
	(*) size, cm	wt, g	wt fraction, %	(*) size, cm	wt, g	wt fraction, %
Anodes	8.0 × 5.0 × 0.004	5.19	7.6	8.0 × 5.0 × 0.004	5.19	21.4
Separators	9.0 × 6.0 × 0.01	6.44	9.4	8.2 × 5.2 × 0.001	0.51	2.1
Liquid electrolyte	25 ml	33.50	48.8	5 ml	6.70	27.7
Cathodes	8.0 × 5.0 × 0.005	6.60	9.6	8.0 × 5.0 × 0.005	6.60	27.3
Anode collectors	10.0 × 5.0 × 0.0025	4.76	7.0	8.5 × 5.0 × 0.001	1.62	6.7
Cathode collectors	10.0 × 5.0 × 0.0025	5.10	7.4	8.5 × 5.0 × 0.001	1.73	7.1
Anode tab	5.0 × 5.0 × 0.003	0.20	0.3	5.0 × 0.5 × 0.002	0.01	0.1
Cathode tab	5.0 × 5.0 × 0.003	0.20	0.3	5.0 × 0.5 × 0.002	0.01	0.1
Package	15.0 × 11.0 × 0.01	6.60	9.6	13.0 × 7.0 × 0.005	1.82	7.5
Final device	12.0 × 6.0 × 0.747	68.59	100.0	9.0 × 5.2 × 0.329	24.19	100
Specific energy, W h kg^{-1}			20.7			58.7 (77.8)***
Volumetric energy, W h dm^{-3}			72.3			93.5 (104.1)***

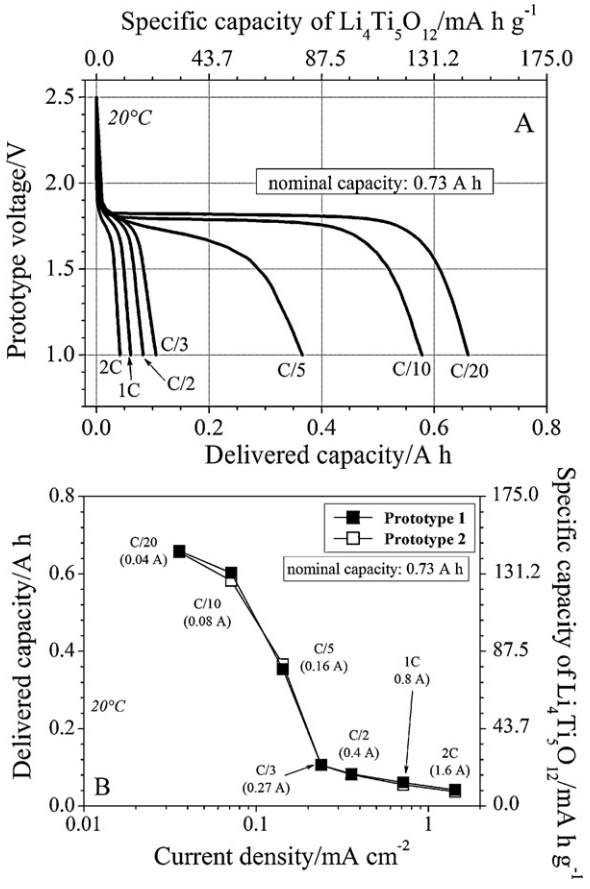

Fig. 5. Voltage vs. discharge capacity profiles (panel A) and discharge capacity vs. current density dependence (panel B) of scaled-up, ionic liquid-based, $Li_4Ti_5O_{12}$/$LiFePO_4$ LIB prototypes. The capacity was also reported with respect to the $Li_4Ti_5O_{12}$ active material weight for comparison purpose. The average discharge current values (and the corresponding discharge rates) are indicated in the panels. T = 20 °C.

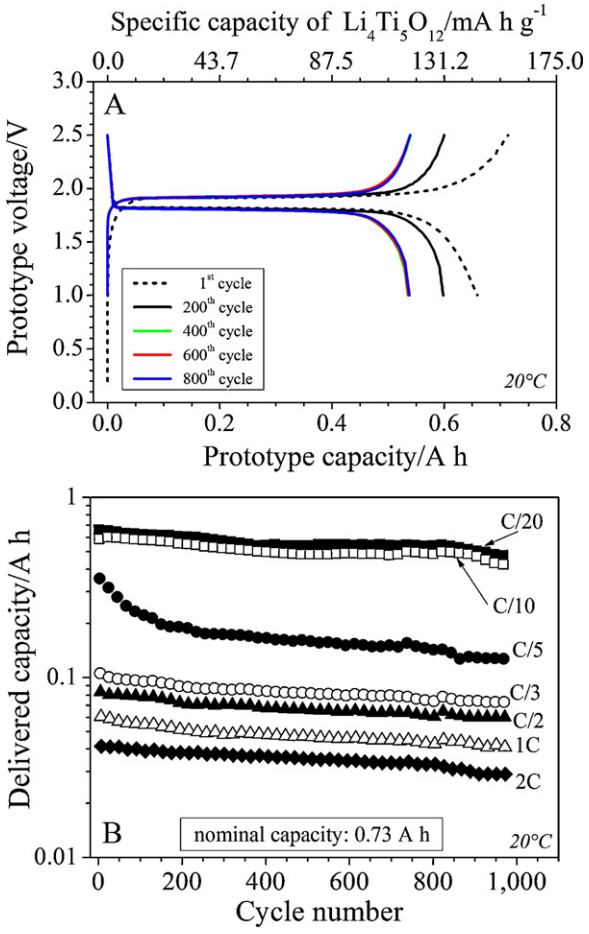

Fig. 6. Voltage vs. capacity profile of selected charge/discharge cycles at C/20 (panel A) and capacity vs. cycle evolution (panel B) of a scaled-up, ionic liquid-based, $Li_4Ti_5O_{12}$/$LiFePO_4$ LIB prototype at different current rates. T = 20 °C.

1.8 V (LIB) the calculated (theoretical) specific and volumetric energies are 54.6 W h kg^{-1} and 69.5 W h dm^{-3} for the LMPB and 20.7 W h kg^{-1} and 72.3 W h dm^{-3} for the LIB prototype. At a first glance, the expected performance of the prototypes is rather limited, however, it is important to notice that the prototypes were realized mainly to prove the feasibility of the cells. The prototypes are very likely subjected to substantial improvement upon industrial production (optimization of each component). For instance, the thickness of each polymer electrolyte layers, which total weight represents about 47% of the device overall weight (Table 1), could be reduced from 100 μm down to 20 ÷ 30 μm using industrial processing. Analogously, thinner (10 ÷ 20 μm) separators could be used for the LIB prototypes, thus lowering the electrolyte weight (presently 58% of the prototype overall weight). Large production volumes would allow to use metal current collectors and tabs of appropriate thickness (totally, 12–15% of the overall weight). Their size and that of the packaging could be easily reduced by 10–15 wt% with the use of state-of-art assembly lines. It is, in fact, important to notice that the active materials (Li or $Li_4Ti_5O_{12}$ and $LiFePO_4$) represented only from 13% to 15% of the prototype overall weight.

Table 4 compares the component characteristics (size, average weight and weight fraction) of the prototypes fabricated as reported in this paper and upon the optimization cited above which would allow to cut the final weight of the devices down to 14.87 g (LMPBs) and 24.19 g (LIBs), respectively, corresponding to an enhancement in (theoretical) gravimetrical and volumetric energy up to 160.1 W h kg^{-1} and 284.1 W h dm^{-3} for the LMPB and 58.7 W h kg^{-1} and 93.5 W h dm^{-3} for the LIB prototype, respectively.

The Ragone plot of the scaled-up Li/$LiFePO_4$ and $Li_4Ti_5O_{12}$/$LiFePO_4$ battery prototypes is displayed in Fig. 7 in terms of gravimetrical energy vs. gravimetrical power (panel A) and volumetric energy vs. volumetric power (panel B). The energy and power data were calculated on the basis of the results obtained from cycling tests but taking into account the prototype optimization described above. On these assumptions, the Li/$LiFePO_4$ prototypes show very interesting energy values approaching 230 W h kg^{-1} and 400 W h dm^{-3}. The $Li_4Ti_5O_{12}$/$LiFePO_4$ prototypes exhibit rather lower energies with respect to the Li/$LiFePO_4$ ones, mainly due to its reduced nominal voltage (1.8 V instead 3.4 V) since the higher intercalation potential of $Li_4Ti_5O_{12}$ (>1.5 V) vs. Li/Li$^+$. However, this prevents lithium plating onto the negative electrode, which, in conjunction with the non-flammability and high stability of the lithium titanium oxide, makes the $Li_4Ti_5O_{12}$/$LiFePO_4$ chemistry appropriate in applications where safety is predominating [29].

To summarize, the Li/$LiFePO_4$ LMPB and $Li_4Ti_5O_{12}$/$LiFePO_4$ LIB prototypes developed in ILLIBATT appear to be appropriate for use in conjunction with photovoltaic panels (PV) where long-term stability and high efficiency, rather than high rate performance, are needed.

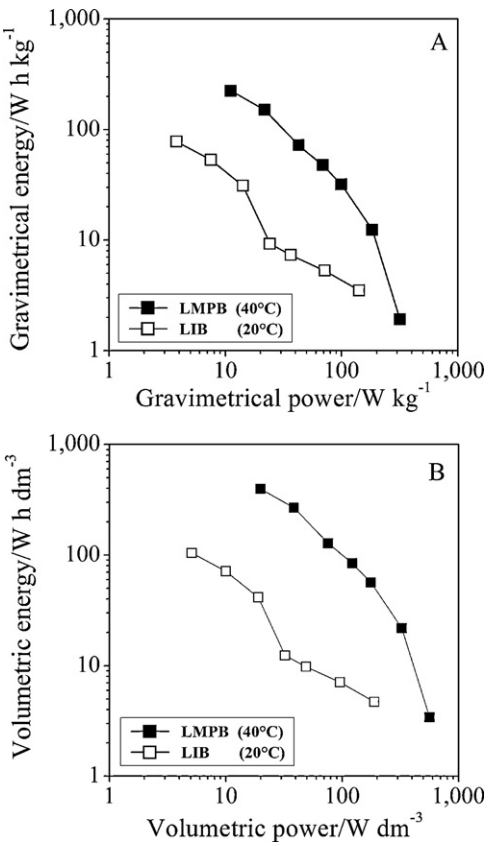

Fig. 7. Ragone plot in terms of gravimetrical energy vs. gravimetrical power (panel A) and volumetric energy vs. volumetric power (panel B) of scaled-up Li/$LiFePO_4$ (LMPB) and $Li_4Ti_5O_{12}$/$LiFePO_4$ (LIB) battery prototypes. The energy and power data were calculated on the basis of the results obtained from cycling tests but taking into accounts on the optimization described in the text.

4. Conclusions

Rechargeable Li/$LiFePO_4$ and $Li_4Ti_5O_{12}$/$LiFePO_4$ cells, based on lithium-conducting, ionic liquid containing, PEO-LiTFSI-PYR_{14}TFSI polymer tape and LiTFSI-PYR_{14}FSI mixture, respectively, as the electrolyte, were scaled-up to fabricate 0.7 A h class, stacked LMPB and LIB prototypes for photovoltaic applications. At C/20, e.g., the current rate required in PV devices, the prototypes have delivered more than 80% of their initial capacity after 800 cycles. Industrial improvements of the active materials, inactive cell components, cell design and manufacturing processes are expected to push the gravimetrical and volumetric energy of the Li/$LiFePO_4$ prototype above 230 W h kg^{-1} and 400 W h dm^{-3}, respectively, whereas, for the $Li_4Ti_5O_{12}$/$LiFePO_4$ prototype, the energy values do not exceed 80 W h kg^{-1} and 105 W h dm^{-3}, respectively.

The moderate rate capability, likely ascribed to diffusive phenomena occurring within the electrolytes, may be enhanced through additional improvement of the preparation route of composite electrodes and of the cell design as well as the utilization of more highly conductive ionic liquids. However, the results evidenced the validity of the organic solvent-free battery chemistry design and the reproducibility of the manufacturing process, thus demonstrating the feasibility of these cell chemistries.

Acknowledgements

The authors gratefully acknowledge the financial support of the European Commission under Contracts NMP3-CT-2006-033181 (ILLIBATT project). Süd Chemie is acknowledged for having provided the active materials.

References

[1] J.R.D. Rogers, K.R. Seddon, Ionic Liquids: Industrial Application to Green Chemistry (ACS Symposium Series 818), American Chemical Society, Washington, 2002.
[2] D.R. MacFarlane, J. Sun, M. Forsyth, P. Meakin, N. Amini, J. Phys. Chem. B 103 (1999) 4164.
[3] G.B. Appetecchi, M. Montanino, D. Zane, M. Carewska, F. Alessandrini, S. Passerini, Electrochim. Acta 54 (2009) 1325.
[4] Q. Zhou, W.A. Henderson, G.B. Appetecchi, M. Montanino, S. Passerini, J. Phys. Chem. B 112 (2008) 13580.
[5] E. Paillard, Q. Zhou, W.A. Henderson, G.B. Appetecchi, M. Montanino, S. Passerini, J. Electrochem. Soc. 156 (2009) A891.
[6] V.R. Koch, NanjundiA. C., G.B. Appetecchi, B. Scrosati, J. Electrochem. Soc. 142 (1995) L116.
[7] D.R. MacFarlane, J. Huang, M. Forsyth, Nature (London) 402 (1999) 792.
[8] G.-T. Kim, G.B. Appetecchi, M. Montanino, F. Alessandrini, S. Passerini, ECS Transactions 25 (36) (2010) 127.
[9] G.B. Appetecchi, M. Montanino, A. Balducci, S.F. Lux, M. Winter, S. Passerini, J. Power Sources 192 (2009) 599.
[10] S.F. Lux, M. Schmuck, G.B. Appetecchi, S. Passerini, M. Winter, A. Balducci, J. Power Sources 192 (2009) 606.
[11] A. Guerfi, S. Duchesne, Y. Kobayashi, A. Vijh, K. Zaghib, J. Power Sources 175 (2008) 866.
[12] T. Sugimoto, Y. Atsumi, M. Kikuta, E. Ishiko, M. Kono, M. Ishikawa, J. Power Sources 189 (2009) 802.
[13] H. Matsumoto, H. Sakaebe, K. Tatsumi, M. Kikuta, E. Ishiko, M. Kono, J. Power Sources 160 (2006) 1308.
[14] G.T. Kim, S.S. Jeong, M. Joost, E. Rocca, M. Winter, S. Passerini, A. Balducci, J. Power Sources 195 (2010) 6130.
[15] S.F. Lux, F. Schappacher, A. Balducci, S. Passerini, J. Electrochem. Soc. 157 (3) (2010) A320.
[16] J.-H. Shin, W.A. Henderson, S. Passerini, Electrochem. Commun. 5 (2003) 1016.
[17] J.-H. Shin, W.A. Henderson, S. Passerini, Electrochem. Solid-state Lett. 8 (2005) 125.
[18] J.-H. Shin, W.A. Henderson, S. Passerini, J. Electrochem. Soc. 152 (2005) A978.
[19] G.-T. Kim, G.B. Appetecchi, F. Alessandrini, S. Passerini, J. Power Sources 171 (2007) 861.
[20] J.-H. Shin, W.A. Henderson, G.B. Appetecchi, F. Alessandrini, S. Passerini, Electrochim. Acta 50 (2005) 3859.
[21] G.B. Appetecchi, G.-T. Kim, M. Montanino, F. Alessandrini, S. Passerini, ECS Transactions 11 (2008) 119.
[22] G.B. Appetecchi, G.T. Kim, M. Montanino, F. Alessandrini, S. Passerini, J. Power Sources 196 (2011) 6703.
[23] G.T. Kim, G.B. Appetecchi, M. Carewska, M. Joost, A. Balducci, M. Winter, S. Passerini, J. Power Sources 195 (2010) 6130.
[24] G.B. Appetecchi, S. Scaccia, C. Tizzani, F. Alessandrini, S. Passerini, J. Electrochem. Soc. 153 (9) (2006) A1685.
[25] G.B. Appetecchi, M. Montanino, M. Carewska, M. Moreno, F. Alessandrini, S. Passerini, Electrochim. Acta 58 (2011) 1300.
[26] P. Villano, M. Carewska, G.B. Appetecchi, S. Passerini, J. Electrochem. Soc. 149 (2002) A1282.
[27] G.B. Appetecchi, Y. Aihara, B. Scrosati, J. Electrochem. Soc. 150 (2003) A301.
[28] G.B. Appetecchi, J.-H. Shin, F. Alessandrini, S. Passerini, J. Power Sources 143 (2005) 236.
[29] B. Scrosati, J. Garche, J. Power Sources 2419 (195) (2010) 9.